IEEE Access
Multidisciplinary | Rapid Review | Open Access Journal

Received 30 June 2024, accepted 15 July 2024, date of publication 22 July 2024, date of current version 5 August 2024.

Digital Object Identifier 10.1109/ACCESS.2024.3432318

RESEARCH ARTICLE

Smartphone-Based Parameter Estimation of the Cole-Impedance Model for Assessment of Agricultural Goods

MITAR SIMIĆ[1], (Senior Member, IEEE), TODD J. FREEBORN[2], (Senior Member, IEEE), AND GORAN M. STOJANOVIĆ[1], (Member, IEEE)

[1]Faculty of Technical Sciences, University of Novi Sad, 21000 Novi Sad, Serbia
[2]Department of Electrical and Computer Engineering, The University of Alabama, Tuscaloosa, AL 35487, USA

Corresponding author: Mitar Simić (mitar.simic@uns.ac.rs)

This work was supported in part by European Union's Horizon 2020 Research and Innovation Program through ERA Chair for emerging technologies and innovative research in Stretchable and Textile Electronics (STRENTEX) Project under Agreement 854194, and in part by the North Atlantic Treaty Organization (NATO) Science for Peace and Security Program through Conductive Composite Based Flexible and Wearable Chemical Sensors (CONSENS) Project under Agreement G6011.

ABSTRACT The Cole-impedance model is extensively utilized for modelling the electrical impedance of biological samples, including agricultural goods (e.g. fruits and vegetables). The conventional methods for estimating parameters of the Cole-impedance model rely on processing multi-frequency impedance datasets using non-linear least squares methods. The quality of the initial value used in these methods has a direct impact on the convergence and estimation accuracy, while requirement for complex processing units lowers portability and *in-situ* applications. This paper introduces method not dependent on a particular platform to estimate parameters of the Cole-impedance model that best represent an impedance dataset, eliminating the need for the specific toolbox within the software package, and it does not necessitate the user to supply initial values. The proposed method is validated using synthetic datasets (with and without noise) and experimental bioimpedance of carrot, potato, and pear samples. Further, it is implemented on a low-cost embedded hardware with execution time <7 seconds (for an impedance dataset with 256 datapoints) and estimation accuracy comparable to PC-based estimations. The embedded hardware is interfaced wirelessly to a smartphone application to demonstrate the *in-situ* graphical evaluation and reporting available using the proposed system.

INDEX TERMS Electrical impedance spectroscopy, Cole-impedance model, fractional-order circuits, parameter estimation, precision agriculture.

I. INTRODUCTION

Electrical Impedance Spectroscopy (EIS) is the technique of measuring the passive electrical properties (typically in resistance/reactance or magnitude/phase formats) of a material over a fixed range of frequencies. This data can inform how the impedance of a material changes with frequency, or how the impedance changes over time due to internal processes of the material or due to ambient conditions. This potential to monitor internal processes in a material motivates the use of this application for characterizing or assessing biological tissues such as agricultural goods [1], [2] and [3], environmental monitoring [4] and membrane fouling detection [5]. Recently EIS has been demonstrated as a potential method for monitoring food freshness and maturity and detecting contamination (such as bacteria or chemicals) in food related products [6]. However, these advances have not yet been translated into commercial application of EIS in agricultural processes. This lack of translation is attributed to limited demonstration of the effectiveness of EIS in real-world agricultural cases to convince farmers and agricultural professionals of how this technique can support their unique needs. Additionally, there has yet to emerge any standardized protocols for EIS measurements and their analysis. This is expected to also limit its adoption due to the complexity of this data and required expertise for proper interpretation (which might be

The associate editor coordinating the review of this manuscript and approving it for publication was Larbi Boubchir.

challenging for many end-users). Therefore, an important step for advancing the adoption of EIS in commercial agricultural applications is the development of data processing methods that are portable, automated, and reliable. These needs for portable, automated, and reliable data processing of EIS data are what motivates this work.

A common approach to EIS data analysis utilizes equivalent electrical circuits to model the underlying physical or physiological processes of the material. With this approach, a multi-frequency dataset (with potentially hundreds of discrete datapoints) can be represented by an electrical circuit model with fewer parameters. The values of the model are selected to accurately represent the experimental data. The particular model can be designed to represent the structural and morphological changes in an analyzed sample [7], [8], which simplifies interpretation by focusing on changes in particular circuit component values as an indicator of the underlying physiological or structural changes. One commonly used equivalent circuit to represent biological tissues is referred to as the Cole-impedance model (discussed with more details in II.A). This model, initially formulated in 1940 [9], has been widely used in assessment of fruits and vegetables. It has four parameters (high frequency resistance R_∞, low frequency resistance R_0, and a fractional-order capacitor with capacitance C and order α) which have been investigated for their relationships with the physiological/structural changes of a range of fruits/vegetables in different conditions. Using this model, the resistances are often attributed to fluids within the tissue and the fractional-order capacitor to the cellular membrane properties. Recently, this model was used with EIS data from *Daucus Carota Sativus* (carrot) samples in freezing and heating conditions [7]. It was reported that R_∞ and R_0 decreased with increasing temperature, which was attributed to increased pectin solubility, but with different rates: R_∞ decreased up to 2.5 times, while R_0 decreased up to 10 times for three analyzed samples. Further, during the freezing treatment both resistances increased due to ice formation, with R_0 having earlier changes than R_∞ due to intracellular structure solubility. These results supported that the intracellular fluid (associated with R_0) of the carrot samples were the parameter most sensitive the temperature increases with potential to track fluid related changes in the tissue samples [7]. Additional studies have also explored the use of the EIS and the Cole-impedance model for the maturity and lifespan estimation of apple, banana, kiwi, carrot, garlic and onion samples [10], [11], and eggplant pulp cellular membrane damage due to drying and freezing–thawing treatments [12]. With the potential for EIS to provide insight regarding the internal tissue properties this technique could be integrated into automated horticulture equipment, such as the robotic equipment demonstrated by Park et al. [13], to further advance precision agriculture.

Successful application of the Cole-impedance model requires reliable and accurate parameter extraction or estimation from the measured EIS dataset. The classical approach utilizes complex nonlinear least squares (CNLS) fitting methods which employ an iterative search for model parameter values. The aim of this search is to identify model values that minimize the error between measured and fitted data [14], [15]. However, CNLS-based methods need an initial guess from which to start the iterative search which is typically provided by the user [16]. There is not a strict rule or criterium which *a priori* defines an initial guess as appropriate because factors such as the fitting algorithm, step size, termination tolerances, number of measurement points, *etc*. all have a direct impact. A common approach is trial and error or random generation of a user-defined ''reasonable'' number of initial values and monitoring of the estimation accuracy [15]. There is also the possibility to have estimation of the initial guess informed by discrete impedance values in the dataset. As an example, R_∞ and R_0 estimates can be generated from the highest and lowest frequency real impedance values, respectively. And an estimate of $\alpha = 0.5$ can be used as a reasonable mid-range value in the range of values (from 0 to 1) possible for a fractional-order capacitor [17], while an initial value of C can be estimated from the imaginary part of impedance at the characteristic frequency [18]. This approach is still sensitive to the highest and lowest frequency datapoints and introduces errors to the R_∞ and R_0 estimates which propagate to errors in the C value estimate which can degrade the fitting performance. Additionally, limitations such as long execution time, dependence on the specific toolbox/function for the efficient implementation and convergence issues have been previously reported when using CNLS-based methods [19]. There are also Cole-impedance estimation methods that do not require direct impedance measurement, which have instead used time domain data [20], [21], or the fractional operational matrix (FOM) [22]. Similar to the direct methods, time-domain methods have used CNLS [21] with algorithms including particle swarm optimization (PSO) [23], [24]. As another iterative process, PSO also have a slow convergence rate [25] which is sensitive to the swarm size and conditions set for the iterative search. Other meta-heuristic optimization techniques, based on single resistor controlled oscillator and flower pollination optimization (FPA) technique, have also been reported [7], [26], [27]. Optimization of FPA for engineering problems is ongoing because of a tendency towards premature convergence and poor exploitation ability [28]. The use of stochastic optimization algorithms, like the bacterial foraging optimization (BFO) algorithm, are other candidates for parameter estimation and have demonstrated improved robustness against noise and higher accuracy when compared to the CNLS method [29]. However, BFO methods also have some drawbacks such as slow convergence speed, being unable to escape from local minima, and having a fixed step length [30]. Machine learning (ML) methods were also recently applied in bioimpedance processing, such as body composition analysis and classifying cellular states [31], transthoracic bioimpedance-based detection of lung fluid accumulation [32], heart failure [33], venous access [34], assessment of knee osteoarthritis

severity [35], bone fractures [36], abnormal tissue detection [37], *etc*. While convolutional neural networks (CNNs) are powerful tools for pattern recognition and classification [34], [36], [37] their application in the context of the Cole-impedance model parameters is expected to require labeled training data and significant computational resources for model training and inference. There is also a requirement for expertise in both electrochemistry and ML for choosing an appropriate algorithm and ensuring its validity. All these limit efficiency and speed for *in-situ* parameter estimation which is an expected requirement for real-time, agricultural processing in the diverse and dynamic conditions typical of harvesting and production environments. Therefore, there is further need to develop rapid and robust parameter estimation techniques for support precision agriculture using EIS data.

The purpose of this paper is to introduce an efficient algorithm for reliable Cole-impedance model parameter estimation from EIS data without user activities (such as data transfer of EIS data to PC-based processing units, data formatting to the specific EIS software, selection and validation of initial values, algorithm selection, step size and termination tolerances definitions, *etc*.) that may impact estimation accuracy. The proposed method eliminates the need for a user to provide initial values, removes the need for specific software functions or toolboxes for processing, and demonstrates faster estimation time and higher estimation accuracy compared to recent relevant works from the literature (discussed with more details in subsection III-D). Most importantly, this estimation method is suitable for low-cost, resource limited microcontroller-based platforms to support *in-situ* applications in precision agriculture (automated selection of ripe fruits, for example). A demonstration of the algorithm is provided using a custom smartphone application which communicates with the microcontroller hardware using the Bluetooth low energy (BLE) protocol, enabling wireless readout and graphical comparison of estimated and measured impedance values. This approach is adopted to support precision agriculture applications in field conditions.

II. MATERIALS AND METHODS

A. THE PROPOSED ESTIMATION METHOD

The Cole-impedance model is an equivalent electrical circuit consisting of three circuit components: two resistors (R_∞ and $R_1 = R_0 - R_\infty$), and a fractional order-capacitor (also referred to as a constant phase element (CPE)) with pseudo-capacitance C and fractional-order $0 \leq \alpha \leq 1$. The physical layout of components and their interconnections are provided in Fig. 1(a). The complex impedance ($\underline{Z}$) at a given angular frequency ω_i [s^{-1}] is described by Equation (1):

$$\underline{Z}(\omega_i) = R(\omega_i) + jX(\omega_i) = R_\infty + \frac{R_1}{1 + R_1 C (j\omega_i)^\alpha} \quad (1)$$

where R represents the real component (or resistance) of the impedance, X represents the imaginary component (or reactance) of the impedance, and i represents the discrete frequency index ranging from 1 to the total number of measured frequencies (N). Equation (2) and Equation (3) provide the analytical expressions for resistance (R) and reactance (X):

$$R(\omega_i) = R_i = R_\infty + \frac{R_1\left(1 + \omega_i^\alpha \cos\left(\frac{\alpha\pi}{2}\right) R_1 C\right)}{\left(1 + \omega_i^\alpha \cos\left(\frac{\alpha\pi}{2}\right) R_1 C\right)^2 + \left(\omega_i^\alpha \sin\left(\frac{\alpha\pi}{2}\right) R_1 C\right)^2} \quad (2)$$

$$X(\omega_i) = X_i = \frac{-\omega_i^\alpha \sin\left(\frac{\alpha\pi}{2}\right) R_1^2 C}{\left(1 + \omega_i^\alpha \cos\left(\frac{\alpha\pi}{2}\right) R_1 C\right)^2 + \left(\omega_i^\alpha \sin\left(\frac{\alpha\pi}{2}\right) R_1 C\right)^2} \quad (3)$$

The presentation of impedance as a Nyquist plot, where resistance is plotted against negative signed reactance (R,-X), provides useful information for data interpretation and estimation of model parameters. For example, the values of resistance at very high and very low frequencies (theoretically) correspond to values of R_∞ and $R_1 + R_\infty$, respectively, when the reactance at the ideal frequencies [$X(f \rightarrow \infty)$ and $X(f = 0)$] are zero. The impact of the parameter α on the resistance and reactance is illustrated in Fig. 1(b). Notice that the resistance at the characteristic frequency, $f_c = 1/[2\pi(R_1 C)^{1/\alpha}]$, remains constant $R_c = R(f_c)$ for decreases in α (in this case decreased from 1 to 0.7 to 0.3), while $X_c = |X(f_c)|$ decreases (observed as a decrease in peak of the arc). Another feature of the data in this format is the impedance phase angle at the characteristic frequency, denoted here as β_c, which is given by Eq. (4):

$$\beta_c = \tan^{-1}\frac{X_c}{R_c} = \frac{R_1 \sin\left(\frac{\alpha\pi}{2}\right)}{(R_1 + 2R_\infty)\left(1 + \cos\left(\frac{\alpha\pi}{2}\right)\right)} \quad (4)$$

The value of β_c is dependent on model parameters R_∞, R_1 and α, while parameter C does not appear in (4). The characteristic angular frequency ω_c can be approximated by identifying the angular frequency at which $|X(\omega_i)|$ reaches its highest value, and knowledge of this value supports the estimation of R_c and X_c from the measurement values.

The estimation method proposed here uses the analytical solution of (2)-(4) with R_i, X_i, α and β_c as input parameters to calculate R_∞, R_1 and C. The detailed analytical solution of (2)-(4) with respect to R_∞, R_1 and C is given as the supplementary material for interested readers. With this derived set of equations, the measured values of R_i, X_i and β_c are used with a linear search (brute force method) to solve for α in the range [0, 1]. The solved value is that which minimizes the mean relative error between measured and estimated resistance and reactance. Fig. 1(c) depicts the flowchart representation of the suggested approach. Additionally, the supplementary materials contain the exact program code for those readers interested in utilizing the proposed method.

B. METHOD VERIFICATION USING SYNTHETIC DATASETS

The proposed method was first validated with synthetic datasets generated using (1) with values $R_\infty = 84.40\ \Omega$, $R_1 = 39.20\ \Omega$, $C = 2.31\ \mu$F and $\alpha = 0.747$ with 256 frequencies spaced logarithmically from 3 kHz to 1 MHz, which are values in the range of tissues when measured with a

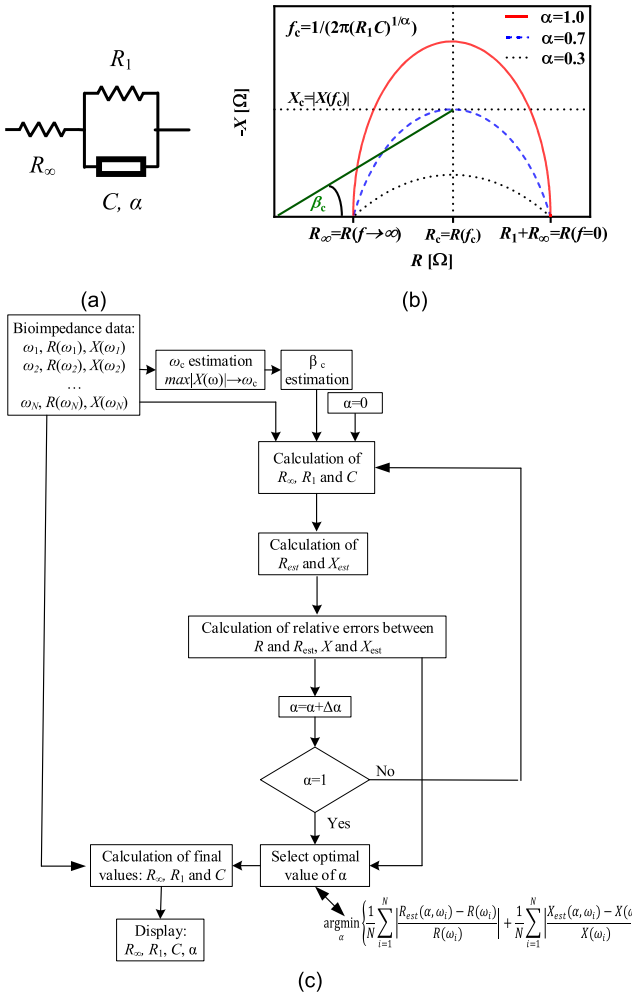

FIGURE 1. **(a) Equivalent electrical circuit of the Cole-impedance model, (b) the typical Nyquist plots for various values of empirical parameter α (other model parameters are constant), (c) the flowchart of the proposed estimation method.**

tetrapolar configuration. In addition to a noiseless dataset (e.g. noise level 0%) datasets with 0.25%, 0.5%, 1.0% and 2.0% random noise (added to both resistance and reactance) were generated to evaluate the impact of noise on the method. The noise levels were based on the expected accuracy of the instrument used in this study to collect experimental data (discussed further in subsection II-C). To evaluate the effect of dataset size on the proposed method datasets with $N = 128$, 64 and 32 (from 3 kHz to 1 MHz) with 1.0% noise were analyzed. Finally, the effect of dataset frequency band on the method was also evaluated using narrower frequency ranges from 3 kHz to 100 kHz (typical of low-cost embedded hardware-based measurement systems using the Analog Devices AD5933 high precision impedance converter integrated circuit) with $N = 16$ and 1% of noise. The mean (μ) and standard deviation (σ) of the Cole-impedance model values were generated from the estimates of 100 repeated applications of the proposed method to each of the generated synthetic datasets. It is important to emphasize that the proposed method will generate the same results ($\sigma = 0$) every time for the same input dataset, but datasets with random noise will yield different values. The relative errors (δ [%]) for mean values compared to the reference value for each model parameters were also calculated.

C. METHOD VERIFICATION USING EXPERIMENTAL DATA

The electrical network shown in Fig. 1(a) was realized using a convenience sample of discrete components with nominal values $R_\infty = 470\ \Omega$, $R_1 = 1000\ \Omega$, $C = 4.7$ nF, and $\alpha = 1$. Tolerances of resistors and capacitors were 5% and 10%, respectively. The electrical impedance of the realized circuit was measured from 1 kHz to 100 kHz with a 1 kHz step size using a PalmSens4 (PalmSens BV, 3995 GA Houten, The Netherlands) impedance instrument. The advertised accuracy of PalmSense4 device from 1 kHz to 100 kHz is >99% for impedances in the range from 10 Ω to 100 kΩ [38].

The electrical impedances of three agricultural products (carrot, potato, and pear) were also collected. Fruits and vegetables were purchased at a local grocer in Novi Sad, Serbia. Samples were washed with tap water and stored for 2 hours at room temperature before measurements. All measurements for carrot and potato were performed using a bipolar electrode configuration with copper wires inserted 10 mm into the vegetables (carrot and potato) reproducing measurement configurations previously reported in the literature [14]. The approximate spacing between electrodes was 8 cm in the case of carrot, and 6 cm in the case of potato. The diameter of the copper wires was 2 mm, which corresponds to AWG 12. The PalmSense4 instrument was utilized for measuring the impedances of carrot and potato with specific configuration: 10 mV sinusoidal excitation voltage, frequency range 1 kHz-1 MHz (logarithmic distribution, 10 points per decade), no DC bias. To highlight that EIS can capture changes over time related to freshness [39], measurements of a pear slice (2.5 cm × 1 cm) using a bipolar platform with gold plated copper electrodes (two parallel strips 40 mm × 5 mm with 14 mm distance and thickness of 2 mm) interfaced to the PalmSense4 (amplitude of voltage 10 mV, 21 logarithmically spaced points in frequency range 2 kHz-200 kHz, with no DC bias) were collected. Pear slices were placed on the top of electrodes, creating a conductive path between them. Measurements were captured immediately after slicing (labelled as "0 h"), followed by measurements after one ("+1 h") and three hours ("+3 h").

D. HARDWARE AND SOFTWARE ESTIMATION PLATFORMS

Initial validation of the proposed method was completed in MATLAB using synthetic datasets. The additive random noise was achieved using the *rng* function with the *Mersenne Twister* algorithm. Next, the proposed method was validated on an Arduino Nano 33 BLE embedded hardware platform. This platform has an ARM Cortex-M4 microcontroller (nRF52840). The nRF52840 has a (default) clock speed of 64 MHz, 1 MB of program memory, and 256 KB of SRAM.

It has a small physical footprint with 45 mm × 18 mm dimensions and weight of 5 grams. The program code for parameter estimation with this hardware platform was developed using the Arduino IDE 1.8.5.

The smartphone application was developed using the MIT App Inventor. The developed application has two modules: one for the BLE communication with the Arduino Nano 33 BLE and the second for presentation of estimated Cole-model values with graphical comparison of measured and estimated impedance. One service (''Cole estimation'') with 8 total characteristics (four Cole-impedance model parameters, measured and estimated resistance and reactance) was implemented, ensuring continuous monitoring of estimated values. After being estimated, characteristics were reported every 1 second. For long-term agriculture applications the sampling time can be increased as changes are expected to occur over hours or days (not seconds). The fast readout was implemented here to validate that the process can be completed in a reasonable time frame. The advantages of the proposed method in which model parameters are estimated on the embedded system and then reported to the smartphone application are: (1) one smartphone can read values from multiple estimation units, (2) smartphone is not needed for the estimation process, enabling the lower overall cost of the system, (3) unsupervised and *in-situ* decision making, and (4) lower energy consumption of the embedded system, which are usually energy-constrained devices, as just four values of model parameters are radio transmitted, rather than entire multi-frequency datasets. A total of $3\times N$ values would need to be transmitted if measured frequencies, real impedances, and imaginary impedances were used for processing on the phone application and not the embedded system.

III. RESULTS AND DISCUSSION

A. THE SYNTHETIC DATASETS: DIFFERENT NOISE LEVELS, NUMBER OF FREQUENCY POINTS AND FREQUENCY RANGE

A summary of the estimated values using synthetic datasets is given in Table 1. For each analysis using the proposed method, a linear sweep with a step size of 0.001 was used for α. The Cole-impedance model parameters were estimated with relatively high accuracy ($\leq$0.07% for R_∞, $\leq$0.36% for R_1, $\leq$0.82% for C, and $\leq$0.07% for α) for all noise levels and number of frequency points in the frequency range 3 kHz-1 MHz. In the reduced frequency range (3 kHz-100 kHz) with just 16 data points and noise level of 1%, the relative errors were 0.16%, 0.36%, 5.84% and 0.57%. The accuracy is worse, that is the average relative error of all 4 estimated model parameters is increased, when the noise level is increased, and the number of measurement points is reduced. For example, in the case of 0% of noise and $N = 256$, the relative errors for R_∞, R_1, C and α were <0.005%, 0.018%, 0.002% and <0.005%, respectively. When noise level is increased to 2% (with $N = 256$), the corresponding relative errors increase to 0.09%, 0.12%, 0.67% and 0.04%. On the other hand, when the number of data points was reduced from 256 to 32 for noise level of 1%, there was an increase of relative errors from 0.04%, 0.06%, 0.38% and 0.03% to 0.07%. 0.09% 0.82% and 0.05%. This is attributed to increased noise shifting values of the real and imaginary impedance at the characteristic frequency from the ideal. This introduces error to the phase angle estimation (β_c) at the characteristic frequency. The proposed method accuracy is very sensitive to the accuracy of this parameter as it is an input parameter for the estimation algorithm. Further, fewer data points can introduce error because the actual value of characteristic frequency is not included (which again impacts the estimation of β_c). As expected, the highest variability was observed for C. This is attributed to the values of C (in the 10^{-6} range) which may introduce numerical errors due to the small values used in the arithmetic operations. It is also

TABLE 1. Estimated values using synthetic datasets with different noise levels, frequency ranges and number of measurement points.

Noise level	Frequency range	N	$R_\infty[\Omega]$ μ±σ	δ [%]
0%	3 kHz-1 MHz	256	84.40	<0.005
0.25%	3 kHz-1 MHz	256	84.39±0.12	0.01
0.5%	3 kHz-1 MHz	256	84.38±0.24	0.02
1.0%	3 kHz-1 MHz	256	84.36±0.47	0.04
2.0%	3 kHz-1 MHz	256	84.33±0.95	0.09
1.0%	3 kHz-1 MHz	128	84.41±0.50	0.01
1.0%	3 kHz-1 MHz	64	84.41±0.51	0.01
1.0%	3 kHz-1 MHz	32	84.34±0.53	0.07
1.0%	3 kHz-0.1 MHz	16	84.27±0.78	0.16
Noise level	Frequency range	N	$R_1[\Omega]$ μ±σ	δ [%]
0%	3 kHz-1 MHz	256	39.21	0.018
0.25%	3 kHz-1 MHz	256	39.19±0.08	0.01
0.5%	3 kHz-1 MHz	256	39.19±0.10	0.02
1.0%	3 kHz-1 MHz	256	39.18±0.17	0.06
2.0%	3 kHz-1 MHz	256	39.15±0.33	0.12
1.0%	3 kHz-1 MHz	128	39.19±0.21	0.04
1.0%	3 kHz-1 MHz	64	39.20±0.21	0.01
1.0%	3 kHz-1 MHz	32	39.17±0.27	0.09
1.0%	3 kHz-0.1 MHz	16	39.34±0.44	0.36
Noise level	Frequency range	N	C[μF] μ±σ	δ [%]
0%	3 kHz-1 MHz	256	2.31	0.002
0.25%	3 kHz-1 MHz	256	2.31±0.05	0.16
0.5%	3 kHz-1 MHz	256	2.31±0.06	0.18
1.0%	3 kHz-1 MHz	256	2.32±0.08	0.38
2.0%	3 kHz-1 MHz	256	2.33±0.13	0.67
1.0%	3 kHz-1 MHz	128	2.33±0.21	0.086
1.0%	3 kHz-1 MHz	64	2.31±0.12	0.03
1.0%	3 kHz-1 MHz	32	2.33±0.16	0.82
1.0%	3 kHz-0.1 MHz	16	2.44±0.45	5.84
Noise level	Frequency range	N	α μ±σ	δ [%]
0%	3 kHz-1 MHz	256	0.747	<0.005
0.25%	3 kHz-1 MHz	256	0.747±0.001	0.012
0.5%	3 kHz-1 MHz	256	0.747±0.001	0.012
1.0%	3 kHz-1 MHz	256	0.747±0.001	0.025
2.0%	3 kHz-1 MHz	256	0.747±0.001	0.040
1.0%	3 kHz-1 MHz	128	0.746±0.001	0.068
1.0%	3 kHz-1 MHz	64	0.747±0.001	0.008
1.0%	3 kHz-1 MHz	32	0.747±0.001	0.050
1.0%	3 kHz-0.1 MHz	16	0.743±0.001	0.573

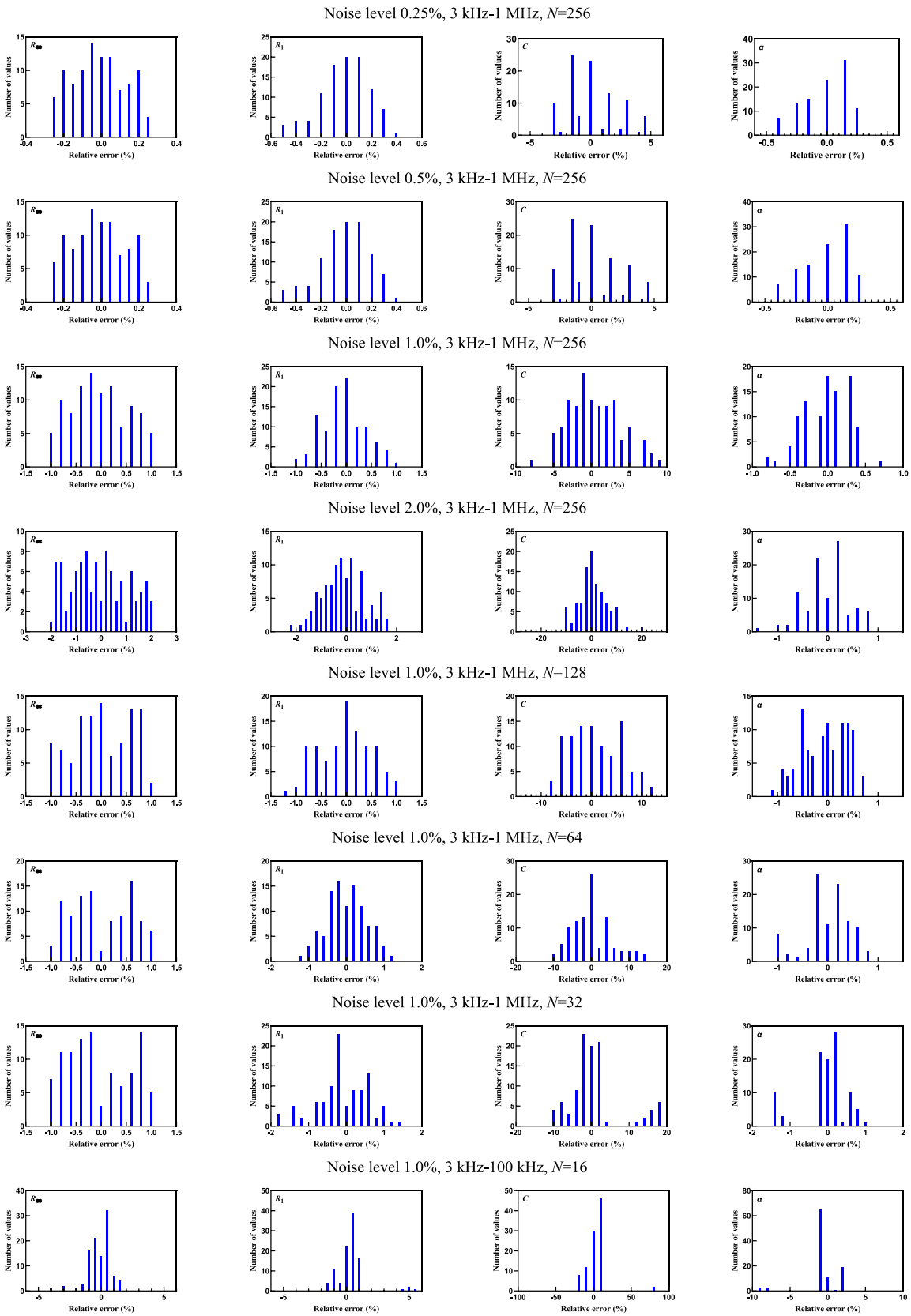

FIGURE 2. The histograms of relative errors for the 100 synthetic datasets with different noise levels (0, 0.25%, 0.5%, 1% and 2.0%), number of frequency points (N=256, 128, 64, 32 and 16) and frequency ranges (3 kHz-1 MHz and 3 kHz-100 kHz).

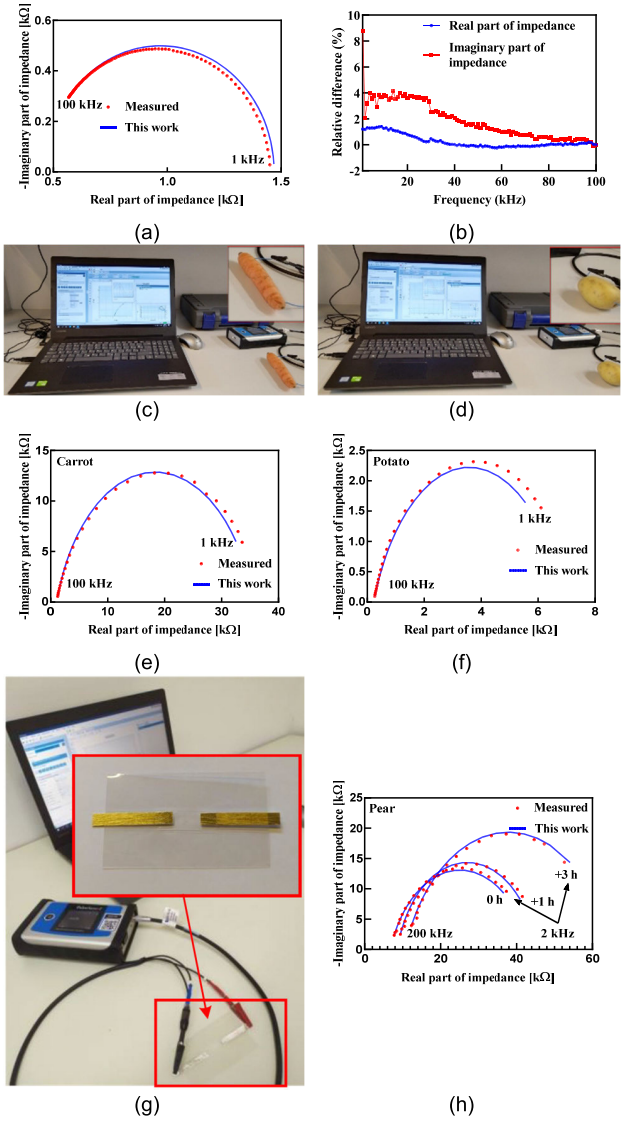

FIGURE 3. (a) Nyquist plots of the measured and estimated impedance values in case of discrete components-based circuit, (b) frequential dependance of relative difference between measured and estimated values (discrete components-based circuit), (c) experimental setup for collecting bioimpedance of carrot, (d) experimental setup for collecting bioimpedance of potato, (e) comparison of experimentally obtained and estimated bioimpedance for carrot, (f) comparison of experimentally obtained and estimated bioimpedance for potato, (g) experimental setup for continuous bioimpedance measurements of pear slices, and (h) comparison of experimentally obtained and estimated bioimpedance of pears slice during the period of 3 hours.

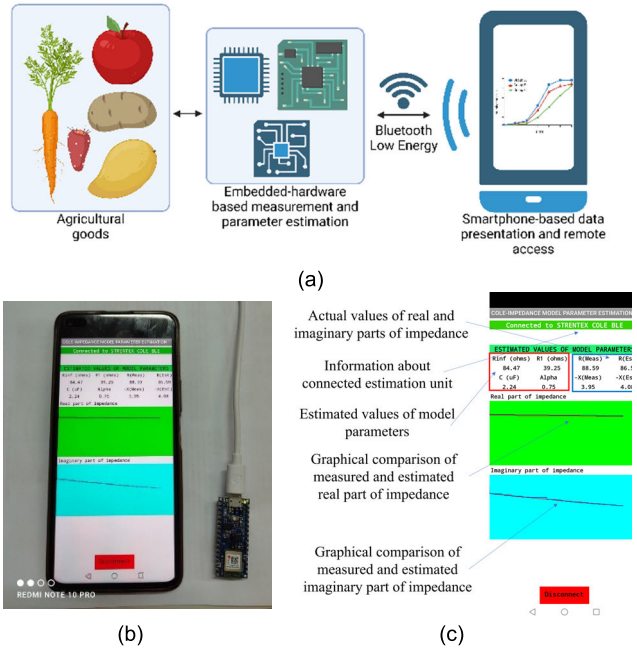

FIGURE 4. (a) Block schematic of smartphone-based EIS analysis, (b) embedded hardware platform and smartphone with installed application for data presentation, (c) main screen of the developed application for Android-based smartphones.

worth mentioning that the analytical solution for parameter C, given by Equation (S3) in the supplementary material, is the most complex and includes the largest number of arithmetic operations (which may increase the accumulation of numerical errors). This sensitivity of the estimation accuracy to low values of C informs a direction of future work beyond the scope of this initial validation.

The histograms, shown in Fig. 2, reveal the frequency distribution of the relative errors for 100 datasets for all four parameters of Cole-impedance model. The relative errors for R_∞ are within the noise level range with similar relative errors for both R_1 and α. The overall estimation accuracy for parameter C is relatively low, with higher than 20% deviation from the expected value. In the context of precision agriculture, physiological features that the Cole model parameters are attributed to are fluid/water content for R_∞ and R_1, the value α characterizes the heterogeneity of samples (which can indicate cell structure changes such as inter-cellular air spaces [7]), and C is often associated with cell membrane properties. Therefore, the proposed method with its current level of variability for estimating the Cole-impedance parameters is most appropriate for monitoring of fluid/water content (but requires further experimental validation).

B. ESTIMATIONS USING THE EXPERIMENTALLY OBTAINED IMPEDANCE

The estimated model parameter values when the proposed method was applied to the EIS data of the discrete components circuit yielded $R_\infty = 471.20\ \Omega$, $R_1 = 998.20\ \Omega$, $C = 4.88$ nF and $\alpha = 1.0$ which show very good agreement with the nominal values ($R_\infty = 470\ \Omega$, $R_1 = 1000\ \Omega$, $C = 4.7$ nF, and $\alpha = 1$) that are within tolerances of the components. Fig. 3(a) provides a graphical comparison between the estimated and measured values, while Fig. 3(b) shows the frequency dependance of relative differences between measured and estimated values. The average relative errors for real and imaginary parts of the impedance are 0.27% and 1.87%, respectively. For reference, the experimental setup for collection of the agricultural samples electrical impedance is shown in Fig. 3(c) and Fig. 3(d). Fig. 3(e) and Fig. 3(f) display the Nyquist plots for both the measured and fitted

values of the carrot and potato samples, respectively. The experimental setup for the measurements of the pear slices is shown in Fig. 3(g), while the comparison of experimental and estimated EIS data during over the 3-hour period is presented in Fig. 3(h).

The estimated values of the Cole-impedance model parameters for the carrot sample are $R_\infty = 1.05$ kΩ, $R_1 = 34.62$ kΩ, $C = 4.93$ nF and $\alpha = 0.814$, with average relative errors for the real and imaginary parts of impedance of 8.75% and 6.70%, respectively. The estimated values of the Cole-impedance model parameters for the potato sample are $R_\infty = 0.22$ kΩ, $R_1 = 6.71$ kΩ, $C = 84.52$ nF and $\alpha = 0.745$. The average relative errors for the real and imaginary parts of impedance for the potato sample are 13.49% and 14.21%, respectively. The estimated values of the Cole-impedance model parameters for the pear slice at 0 hours are: $R_\infty = 6.80$ kΩ, $R_1 = 36.61$ kΩ, $C = 5.75$ nF and $\alpha = 0.791$ (with average relative errors for real and imaginary part of impedance of 4.52% and 4.68%, respectively). After one hour (+1 h), the values were: $R_\infty = 8.60$ kΩ, $R_1 = 36.85$ kΩ, $C = 2.67$ nF and $\alpha = 0.843$ (with average relative errors for real and imaginary part of impedance: 3.91% and 3.24%, respectively). After three hours (+3 h), the values were: $R_\infty = 10.61$ kΩ, $R_1 = 54.53$ kΩ, $C = 3.63$ nF and $\alpha = 0.786$ (with average relative errors for real and imaginary part of impedance: 2.39% and 4.57%, respectively). Notice that there is an increase in the R_∞ and R_1 values of the pear slice over time, which is attributed to the evaporation or loss of water content over time for this sample. There is also a decrease of capacitance C over this same period, while α varied around 0.8.

The average relative errors for the pear slice are less than the samples of carrot and potato, which may be attributed to the sample size/preparation (e.g. a pear slice in comparison to a complete carrot or potato sample) which is expected to give better homogeneity of the sample. Additionally, the overlapping area of the pear slice with the gold electrodes is approximately 0.75 cm on both electrodes, which is larger than the cross section and thickness of the copper wires inserted into the carrot and potato. This may result in lower contact impedance for the pear slice which may also impact data accuracy (but requires further investigation to confirm).

C. PROPOSED METHOD DEPLOYMENT ON EMBEDDED HARDWARE WITH SMARTPHONE CONNECTIVITY

The proposed estimation method was implemented on the Arduino Nano 33 BLE platform (described previously in Section II-D). The code used 116800 of 983040 bytes, which is less than 11% of the available flash memory resources. The global variables required 62600 of 262144 bytes, which is less than 23% of available RAM. When using the Arduino Nano 33 BLE platform and our program code for the parameter estimation with the 0.25% noise, the same results as in the MATLAB-based implementation were achieved. The microcontroller-based parameter estimation required

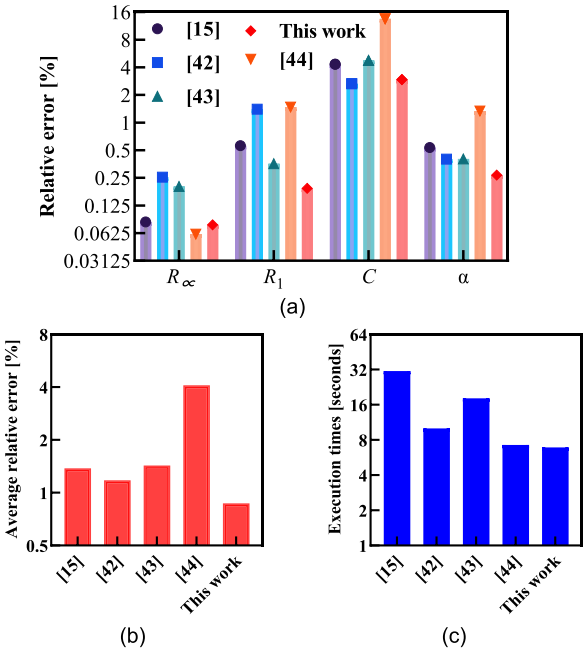

FIGURE 5. Comparison of proposed method with the relevant references in terms of: (a) estimation accuracy, (b) average relative errors and (c) execution time.

6.90 seconds supporting that reliable and stable estimations are possible using a standard C/C++ compiler and inexpensive 32-bit microcontroller.

An important feature highlighted in this system is the centralized graphical display of estimated values and *in-situ* assessment of estimation accuracy which is shown in Fig. 4(a). The wireless functionality of the Arduino Nano 33 BLE with the developed application for Android-based smartphones, shown in Fig. 4(b), supports the rapid review of collected and analyzed measurements. A screenshot of the main window of the smartphone application showing the pilot interface to report impedance and estimated values collected over time in Fig. 4(c). This system architecture can also support multiple estimation units, though the current application is limited to one connected device. It is expected that the maximum number of devices that can be included, which is influenced by connection parameters, network architecture, and device characteristics, will be 10 or less [40].

The reported current consumption at peak power of the nRF52840 is approximately 15 mA [41], but the actual power consumption depends on multiple factors including the number of attached peripherals and code optimizations.

D. COMPARISON OF THE PROPOSED ESTIMATION METHOD WITH THE RELEVANT WORKS FROM THE LITERATURE

Three techniques for estimating the parameters of the Cole-impedance model using embedded hardware and EIS data have been recently published [42], [43], and [44]. The first method involves utilizing measured values of the real and imaginary components of impedance with a

TABLE 2. Evaluating the proposed method in contrast to the relevant literature.

Ref, year	Method	Limitations	This Contribution
[14], 2017 [15], 2019	Complex nonlinear least squares (CNLS)	• CNLS-based methods need a very good initial guess, • long execution time, • dependence on the specific toolbox/function for the efficient implementation, and • convergence issues.	Our method eliminates the need for the user to provide initial values, or inclusion of any specific function or toolbox.
[20], 2022 [22], 2020 [45], 2019 [46], 2010 [47], 2012 [48], 2015 [49], 2018 [50], 2011	Time-domain and indirect measurements	• Time-domain methods are usually used in combination with the CNLS fitting, and • indirect measurements may require very specific hardware to collect data in the proper manner.	Our estimation method works with measured values of complex impedance, obtained with the classic procedures, eliminating the need for any specialized hardware.
[23], 2021 [24], 2021	Particle swarm optimization (PSO)	• Possibility to fall into local minimum, and • the iterative process has a slow convergence rate.	Our method is not iterative.
[26], 2019 [28], 2018	Meta-heuristic optimization techniques	• tendency towards premature convergence, and • poor exploitation ability.	Our method is not subject to non-convergence issues.
[29], 2016	Bacterial foraging optimization (BFO) algorithm	• slow convergence speed, • easy to fail in the local optima, and • a fixed step length.	Our method is not subject to non-convergence issues and local minimum optimizations.

numerical approximation of their quotient's first derivative and was tested on a Raspberry Pi Pico [42]. The second method is based on processing R, X and R_c and was tested on a ATmega2560-based platform [43]. Another ATmega2560-based estimation method used the characteristic frequency ω_c and the corresponding real and imaginary components of the impedance at this frequency (R_c and X_c) [44]. The novelty and contribution of the method proposed in this paper is the reduced computational complexity in comparison to [42] because the numerical approximation of first derivative of R/X quotient is not required. Further, the presented estimation method uses the complete set of real and imaginary impedance (R and X) and β_c (which incorporates both R_c and X_c) which improves the estimation accuracy when compared to [43] and [44]. When compared to previous work that uses a CNLS implemented on an embedded-hardware platform (Raspberry Pi 3) [15], this work does not need the software environment/libraries (SciPy within Python) and does not require a random generation of initial values of model parameters for the iterative searches.

To evaluate how the proposed method compares to previously published methods, in terms of accuracy and execution time, the previously reported performance data for similar synthetic datasets (3 kHz-1 MHz, $N = 256$, 0.25% noise) is compared to the values in this work. The relative errors of each parameter using the described methods are given in Fig. 5(a) with the overall relative errors given in Fig. 5(b). Note that these values were generated on different embedded-hardware platforms (Raspberry Pi 3 [15], Raspberry Pi Pico [42], and ATmega2560-based [43] and [44]) than Arduino Nano 33 BLE used in this work. Therefore, this is a comparison of not just the proposed algorithm but the algorithm/hardware combination. From the values given in Fig. 5(a) the proposed method has the smallest relative error for all parameters except R_∞, for which only [44] was slightly better. However, the average relative error for all four parameters was the lowest with the proposed method (0.87%), as shown in Fig. 5(b). The proposed method also had the lowest execution time (6.90 seconds), as shown in Fig.5(c). This supports that this method does have lower numerical complexity in comparison to previously proposed methods which results in faster execution time.

While this proposed method is best compared against similar numerical approaches designed for low-resource embedded hardware, a further high-level comparison of this work to other EIS-based parameter estimation methods is provided in Table 2. This table summarizes recent CNLS, indirect methods, and optimization methods along with their limitations and the specific contributions of this proposed work to advance beyond those limitations.

IV. CONCLUSION

This article introduces a new technique for estimating the parameters of the Cole-impedance model using the real and imaginary components of impedance measurements in combination with the impedance phase angle value at the characteristic frequency and linear sweep search. This proposed method has lower numerical complexity in comparison to recent estimation techniques and does not require the use of extensive software libraries. This makes it a strong

candidate for on-board Cole-impedance model estimation on low-resource embedded hardware which has the potential to support precision agriculture applications. Our method is not platform-dependent, which reduces dependency on an integrated impedance measurement system. Therefore, the system is capable of processing and analyzing data from various sources, which supports offline EIS analysis. Accurate estimation of the Cole-impedance model parameters from EIS data of carrot, potato and pear samples illustrates the application of this method with reporting and control by a smartphone application to highlight the usability and visualization opportunities available using the proposed system architecture.

The applicability of the proposed method is limited to the EIS spectrum that includes the characteristic frequency, or a measurement point that is close to that value. That has an impact on the estimation accuracy of the characteristic phase angle β_c with Eq. (4), as it is affected by the deviation of the frequency point at which imaginary part has the maximum from the actual characteristic frequency.

Our future efforts will explore creating an impedance measurement device with a 4-electrode configuration that directly estimates *in-situ* the Cole-impedance model parameters to support studies beyond laboratory environments. Moreover, implementation of the machine learning methods is a very interesting topic, especially with the tinyML approach.

SUPPLEMENTARY MATERIALS

The detailed analytical solution of (2)-(4) with respect to R_∞, R_1 and C is given as Supplementary materials. Additionally, the supplementary materials contain the exact program code for utilization of the proposed method.

REFERENCES

[1] J. Cheng, P. Yu, Y. Huang, G. Zhang, C. Lu, and X. Jiang, "Application status and prospect of impedance spectroscopy in agricultural product quality detection," *Agriculture*, vol. 12, no. 10, p. 1525, Sep. 2022, doi: 10.3390/agriculture12101525.

[2] P. Ibba, A. Falco, B. D. Abera, G. Cantarella, L. Petti, and P. Lugli, "Bio-impedance and circuit parameters: An analysis for tracking fruit ripening," *Postharvest Biol. Technol.*, vol. 159, Jan. 2020, Art. no. 110978.

[3] Y. Liu, D. Li, J. Qian, B. Di, G. Zhang, and Z. Ren, "Electrical impedance spectroscopy (EIS) in plant roots research: A review," *Plant Methods*, vol. 17, no. 1, p. 118, Nov. 2021, doi: 10.1186/s13007-021-00817-3.

[4] R. Saha, N. Katiyar, S. Sarma Choudhury, and K. Manoharan, "Impedance spectroscopy and environmental monitoring," in *Impedance Spectroscopy and Its Application in Biological Detection*, 1st ed., Boca Raton, FL, USA: CRC Press, 2023, pp. 79–106, doi: 10.1201/9781003358091-7.

[5] G. L. Goh, M. F. Tay, J. M. Lee, J. S. Ho, L. N. Sim, W. Y. Yeong, and T. H. Chong, "Potential of printed electrodes for electrochemical impedance spectroscopy (EIS): Toward membrane fouling detection," *Adv. Electron. Mater.*, vol. 7, no. 10, Oct. 2021, Art. no. 2100043, doi: 10.1002/aelm.202100043.

[6] M. El-Azazy, "Electrochemical impedance spectroscopy (EIS) in food, water, and drug analyses: Recent advances and applications," in *Electrochemical Impedance Spectroscopy*, M. El-Azazy, M. Min, and P. Annus, Eds., London, U.K.: IntechOpen, 2020, doi: 10.5772/intechopen.92333.

[7] B. M. Aboalnaga, L. A. Said, A. H. Madian, A. S. Elwakil, and A. G. Radwan, "Cole bio-impedance model variations in *Daucus~Carota~Sativus* under heating and freezing conditions," *IEEE Access*, vol. 7, pp. 113254–113263, 2019, doi: 10.1109/ACCESS.2019.2934322.

[8] D. A. Dean, T. Ramanathan, D. Machado, and R. Sundararajan, "Electrical impedance spectroscopy study of biological tissues," *J. Electrostatics*, vol. 66, nos. 3–4, pp. 165–177, Mar. 2008, doi: 10.1016/j.elstat.2007.11.005.

[9] K. S. Cole, "Permeability and impermeability of cell membranes for ions," in *Proc. Cold Spring Harbor Symp. Quant. Biol.*, Jan. 1940, pp. 110–122, doi: 10.1101/SQB.1940.008.01.013.

[10] I. S. Jesus, J. A. T. Machado, and J. B. Cunha, "Fractional electrical impedances in botanical elements," *J. Vibrat. Control*, vol. 14, nos. 9–10, pp. 1389–1402, Sep. 2008.

[11] I. S. Jesus and J. A. T. Machado, "Application of integer and fractional models in electrochemical systems," *Math. Problems Eng.*, vol. 2012, no. 1, pp. 1–17, Jan. 2012, doi: 10.1155/2012/248175.

[12] L. Wu, Y. Ogawa, and A. Tagawa, "Electrical impedance spectroscopy analysis of eggplant pulp and effects of drying and freezing–thawing treatments on its impedance characteristics," *J. Food Eng.*, vol. 87, no. 2, pp. 274–280, Jul. 2008, doi: 10.1016/j.jfoodeng.2007.12.003.

[13] Y. Park, J. Seol, J. Pak, Y. Jo, J. Jun, and H. I. Son, "A novel end-effector for a fruit and vegetable harvesting robot: Mechanism and field experiment," *Precis. Agricult.*, vol. 24, no. 3, pp. 948–970, Jun. 2023, doi: 10.1007/s11119-022-09981-5.

[14] T. J. Freeborn, A. S. Elwakil, and B. Maundy, "Variability of Cole-model bioimpedance parameters using magnitude-only measurements of apples from a two-electrode configuration," *Int. J. Food Properties*, vol. 20, pp. 507–519, Dec. 2017, doi: 10.1080/10942912.2017.1300810.

[15] T. J. Freeborn, "Performance evaluation of raspberry Pi platform for bioimpedance analysis using least squares optimization," *Pers. Ubiquitous Comput.*, vol. 23, no. 2, pp. 279–285, Apr. 2019, doi: 10.1007/s00779-019-01203-6.

[16] M. Žic, "Solving CNLS problems by using Levenberg–Marquardt algorithm: A new approach to avoid off-limits values during a fit," *J. Electroanal. Chem.*, vol. 799, pp. 242–248, Aug. 2017, doi: 10.1016/j.jelechem.2017.06.008.

[17] T. J. Freeborn, "A survey of fractional-order circuit models for biology and biomedicine," *IEEE J. Emerg. Sel. Topics Circuits Syst.*, vol. 3, no. 3, pp. 416–424, Sep. 2013, doi: 10.1109/JETCAS.2013.2265797.

[18] J. Sihvo, T. Roinila, and D.-I. Stroe, "Novel fitting algorithm for parametrization of equivalent circuit model of Li-ion battery from broadband impedance measurements," *IEEE Trans. Ind. Electron.*, vol. 68, no. 6, pp. 4916–4926, Jun. 2021, doi: 10.1109/TIE.2020.2988235.

[19] B. Sanchez, A. S. Bandarenka, G. Vandersteen, J. Schoukens, and R. Bragos, "Novel approach of processing electrical bioimpedance data using differential impedance analysis," *Med. Eng. Phys.*, vol. 35, no. 9, pp. 1349–1357, Sep. 2013, doi: 10.1016/j.medengphy.2013.03.006.

[20] D. Kubanek, J. Koton, and O. Svecova, "Extraction of cardiac cell membrane fractional-order capacitance from current response to voltage step," *Elektronika Ir Elektrotechnika*, vol. 28, no. 4, pp. 42–47, Aug. 2022, doi: 10.5755/j02.eie.31151.

[21] T. J. Freeborn, B. Maundy, and A. S. Elwakil, "Cole impedance extractions from the step-response of a current excited fruit sample," *Comput. Electron. Agricult.*, vol. 98, pp. 100–108, Oct. 2013, doi: 10.1016/j.compag.2013.07.017.

[22] F. Zhang, Z. Teng, S. Rutkove, Y. Yang, and J. Li, "A simplified time-domain fitting method based on fractional operational matrix for Cole parameter estimation," *IEEE Trans. Instrum. Meas.*, vol. 69, no. 4, pp. 1566–1575, Apr. 2020, doi: 10.1109/TIM.2019.2912592.

[23] Á. Odry, Z. Vizvari, N. Gyorfi, L. Kovács, G. Eigner, M. Klincsik, Z. Sari, P. Odry, and A. Toth, "Application of heuristic optimization in bioimpedance spectroscopy evaluation," in *Proc. IEEE 15th Int. Symp. Appl. Comput. Intell. Informat. (SACI)*, Timisoara, Romania, May 2021, pp. 105–112, doi: 10.1109/SACI51354.2021.9465617.

[24] T. J. Freeborn and S. Critcher, "Estimating Cole-impedance parameters from limited frequency-band impedance measurements," in *Proc. IEEE 12th Latin Amer. Symp. Circuits Syst. (LASCAS)*, Arequipa, Peru, Feb. 2021, pp. 1–4, doi: 10.1109/LASCAS51355.2021.9459167.

[25] M. Li, W. Du, and F. Nian, "An adaptive particle swarm optimization algorithm based on directed weighted complex network," *Math. Problems Eng.*, vol. 2014, pp. 1–7, Jan. 2014, doi: 10.1155/2014/434972.

[26] M. Mohsen, L. A. Said, A. H. Madian, A. S. Elwakil, and A. G. Radwan, "Using meta-heuristic optimization to extract bio-impedance parameters from an oscillator circuit," in *Proc. 17th IEEE Int. New Circuits Syst. Conf. (NEWCAS)*, Munich, Germany, Jun. 2019, pp. 1–4, doi: 10.1109/NEWCAS44328.2019.8961229.

[27] S. Kapoulea, A. M. AbdelAty, A. S. Elwakil, C. Psychalinos, and A. G. Radwan, "Cole-Cole bio-impedance parameters extraction from a single time-domain measurement," in *Proc. 8th Int. Conf. Modern Circuits Syst. Technol. (MOCAST)*, May 2019, pp. 1–4.
[28] W. Cui and Y. He, "Biological flower pollination algorithm with orthogonal learning strategy and catfish effect mechanism for global optimization problems," *Math. Problems Eng.*, vol. 2018, pp. 1–16, Jan. 2018, doi: 10.1155/2018/6906295.
[29] S. Gholami-Boroujeny and M. Bolic, "Extraction of Cole parameters from the electrical bioimpedance spectrum using stochastic optimization algorithms," *Med. Biol. Eng. Comput.*, vol. 54, no. 4, pp. 643–651, Apr. 2016, doi: 10.1007/s11517-015-1355-y.
[30] H. Chen, Q. Zhang, J. Luo, Y. Xu, and X. Zhang, "An enhanced bacterial foraging optimization and its application for training kernel extreme learning machine," *Appl. Soft Comput.*, vol. 86, Jan. 2020, Art. no. 105884, doi: 10.1016/j.asoc.2019.105884.
[31] K. Tara and M. H. Islam, "Machine-learning models for detection of cellular states of human body using bio-impedance spectroscopy," *Sens. Bio-Sens. Res.*, vol. 44, Jun. 2024, Art. no. 100648, doi: 10.1016/j.sbsr.2024.100648.
[32] N. Reljin, H. F. Posada-Quintero, C. Eaton-Robb, S. Binici, E. Ensom, E. Ding, A. Hayes, J. Riistama, C. Darling, D. Mcmanus, and K. H. Chon, "Machine learning model based on transthoracic bioimpedance and heart rate variability for lung fluid accumulation detection: Prospective clinical study," *JMIR Med. Informat.*, vol. 8, no. 8, Aug. 2020, Art. no. e18715, doi: 10.2196/18715.
[33] D. Lindholm, E. Fukaya, N. J. Leeper, and E. Ingelsson, "Bioimpedance and new-onset heart failure: A longitudinal study of >500 000 individuals from the general population," *J. Amer. Heart Assoc.*, vol. 7, no. 13, Jul. 2018, Art. no. e008970, doi: 10.1161/jaha.118.008970.
[34] M. Koskinopoulou, A. Acemoglu, V. Penza, and L. S. Mattos, "Dual robot collaborative system for autonomous venous access based on ultrasound and bioimpedance sensing technology," in *Proc. IEEE Int. Conf. Robot. Autom. (ICRA)*, London, U.K., May 2023, pp. 4648–4653, doi: 10.1109/ICRA48891.2023.10160848.
[35] J. D. Muñoz, V. H. Mosquera, C. F. Rengifo, and E. Roldan, "Machine learning-based bioimpedance assessment of knee osteoarthritis severity," *Biomed. Phys. Eng. Exp.*, vol. 10, no. 4, Jul. 2024, Art. no. 045013, doi: 10.1088/2057-1976/ad43ef.
[36] Q. Hua, Y. Li, M. W. Frost, S. Kold, O. Rahbek, and M. Shen, "Machine learning-assisted equivalent circuit characterization for electrical impedance spectroscopy measurements of bone fractures," *IEEE Trans. Instrum. Meas.*, vol. 73, pp. 1–15, 2024, doi: 10.1109/TIM.2024.3350117.
[37] V. Penza, Z. Cheng, M. Koskinopoulou, A. Acemoglu, D. G. Caldwell, and L. S. Mattos, "Vision-guided autonomous robotic electrical bio-impedance scanning system for abnormal tissue detection," *IEEE Trans. Med. Robot. Bionics*, vol. 3, no. 4, pp. 866–877, Nov. 2021, doi: 10.1109/TMRB.2021.3098938.
[38] *Potentiostat / Galvanostat / Impedance Analyzer (PalmSens4)*. Accessed: Jun. 30, 2024. [Online]. Available: https://www.palmsens.com/product/palmsens4/
[39] T. Kojic, M. Simic, M. Pojic, and G. M. Stojanovic, "Detecting freshness of fruit and vegetable without and with edible protein-based foil," *IEEE Sensors J.*, vol. 22, no. 16, pp. 15698–15705, Aug. 2022, doi: 10.1109/JSEN.2022.3188388.
[40] J. Tosi, F. Taffoni, M. Santacatterina, R. Sannino, and D. Formica, "Performance evaluation of Bluetooth low energy: A systematic review," *Sensors*, vol. 17, no. 12, p. 2898, Dec. 2017, doi: 10.3390/s17122898.
[41] *What You Should Know About Bluetooth NRF52832 Beacon*. Accessed: Jun. 30, 2024. [Online]. Available: https://www.mokoblue.com/nrf52832-beacon/
[42] M. Simić, T. J. Freeborn, T. B. Sekara, A. K. Stavrakis, V. Jeoti, and G. M. Stojanović, "A novel method for in-situ extracting bio-impedance model parameters optimized for embedded hardware," *Sci. Rep.*, vol. 13, no. 1, p. 5070, Mar. 2023, doi: 10.1038/s41598-023-31860-w.
[43] M. Simic, T. J. Freeborn, M. Veletic, F. Seoane, and G. M. Stojanovic, "Parameter estimation of the single-dispersion fractional Cole-impedance model with the embedded hardware," *IEEE Sensors J.*, vol. 23, no. 12, pp. 12978–12987, Jun. 2023, doi: 10.1109/JSEN.2023.3269952.
[44] M. Simić, V. Jeoti, and G. M. Stojanović, "Parameter extraction of the Cole-impedance model for in-situ monitoring of electrochemical sources," *J. Energy Storage*, vol. 77, Jan. 2024, Art. no. 109895.
[45] C. Vastarouchas, C. Psychalinos, A. S. Elwakil, and A. A. Al-Ali, "Novel two-measurements-only Cole-Cole bio-impedance parameters extraction technique," *Measurement*, vol. 131, pp. 394–399, Jan. 2019.
[46] A. S. Elwakil and B. Maundy, "Extracting the Cole-Cole impedance model parameters without direct impedance measurement," *Electron. Lett.*, vol. 46, no. 20, p. 1367, 2010, doi: 10.1049/el.2010.1924.
[47] B. Maundy and A. S. Elwakil, "Extracting single dispersion Cole–Cole impedance model parameters using an integrator setup," *Anal. Integr. Circuits Signal Process.*, vol. 71, no. 1, pp. 107–110, Apr. 2012, doi: 10.1007/s10470-011-9751-1.
[48] B. J. Maundy, A. S. Elwakil, and A. Allagui, "Extracting the parameters of the single-dispersion Cole bioimpedance model using a magnitude-only method," *Comput. Electron. Agricult.*, vol. 119, pp. 153–157, Nov. 2015, doi: 10.1016/j.compag.2015.10.014.
[49] C. Vastarouchas, G. Tsirimokou, and C. Psychalinos, "Extraction of Cole-Cole model parameters through low-frequency measurements," *AEU-Int. J. Electron. Commun.*, vol. 84, pp. 355–359, Feb. 2018, doi: 10.1016/j.aeue.2017.11.020.
[50] T. J. Freeborn, B. Maundy, and A. Elwakil, "Numerical extraction of Cole-Cole impedance parameters from step response," *Nonlinear Theory Appl., IEICE*, vol. 2, no. 4, pp. 548–561, 2011, doi: 10.1587/nolta.2.548.

MITAR SIMIĆ (Senior Member, IEEE) was born in Ljubovija, Serbia, in 1987. He received the B.Sc. and M.Sc. degrees in electrical engineering from the University of East Sarajevo, Republika Srpska, Bosnia and Herzegovina, in 2010 and 2012, respectively, and the Ph.D. degree in electrical engineering from the University of Novi Sad, Serbia, in 2017.

He is currently a Postdoctoral Researcher with the STRENTEX Project, Faculty of Technical Sciences, University of Novi Sad. He is the author/coauthor of 45 scientific articles in leading peer-reviewed journals with impact factor. His research interests include sensors, impedance spectroscopy analysis, equivalent circuit modeling, and development of devices for impedance measurement and data acquisition.

TODD J. FREEBORN (Senior Member, IEEE) received the B.Sc., M.Sc., and Ph.D. degrees in electrical engineering from the University of Calgary, Calgary, AB, Canada, in 2008, 2010, and 2014, respectively.

Since 2015, he has been with the Department of Electrical and Computer Engineering, The University of Alabama, Tuscaloosa, AL, USA. He is currently an Associate Professor. His research interests include characterizing changes in biological tissues using their electrical impedance, application of fractional-order models to biological tissues, and the design of fractional-order circuits and systems.

GORAN M. STOJANOVIĆ (Member, IEEE) received the B.Sc., M.Sc., and Ph.D. degrees in electrical engineering from the Faculty of Technical Sciences (FTS), University of Novi Sad (UNS), Serbia, in 1996, 2003, and 2005, respectively.

He has been a Supervisor of 14 Ph.D. students, 40 M.Sc. students, and 60 Diploma students with FTS-UNS. He is currently a Full Professor with FTS-UNS. He has 27 years of experience in research and development. He is the author/coauthor of 280 articles, including 161 in peer-reviewed journals with impact factors, five books, three patents, and two chapters in monographs. He was a keynote speaker for 14 international conferences. He has more than 18 years' experience in coordination of EU funded projects (Horizon Europe, H2020, FP7, EUREKA, and ERASMUS), with a total budget exceeding 21.86 MEUR. He coordinates five Horizon projects in the field of green electronics and textile electronics. His research interests include sensors, flexible electronics, textile electronics, and microfluidics.